International Journal of Steel Structures 18(1): 163-177 (2018)
DOI 10.1007/s13296-018-0313-6
ISSN 1598-2351 (Print)
ISSN 2093-6311 (Online)

International Journal of
STEEL
STRUCTURES
www.springer.com/journal/13296

Investigation of Proposed Concrete Filled Steel Tube Connections under Reversed Cyclic Loading

Farhad Ahadi Koloo[1], Armin Badakhshan[2], Hossein Fallahnejad[3], Mehdi Ebadi Jamkhaneh[4,*], and Masoud Ahmadi[4]

[1]*Aerospace Engineering faculty, Tehran University, Iran*
[2]*Faculty of Civil Engineering, Shahrood University of technology, Iran*
[3]*Department of Civil Engineering, Babol University of technology, Iran*
[4]*Faculty of Civil Engineering, Semnan University, Semnan, Iran*

Abstract

Concrete-filled steel tube (CFT) columns are used in the primary lateral resistance systems. The objective of this research is to analyse the behavior of the steel beam to CFT column connections. A three-dimensional numerical model for simulating the behavior of CFT connections was developed with the aid of the general purpose nonlinear finite element analysis package ABAQUS. In this paper, 90 CFT connection specimens include simple and moment connections that were tested under reversed cyclic loading. Shear capacity of joint, moment-drift response, energy absorption, and displacement ductility were studied in those models. The results have indicated that, the hysteresis curve of CFT columns was plump; no pinch phenomenon can be found; the damage and degradation degree of the strength and stiffness of specimens is lower; and high energy dissipation capacity can be achieved. Improvement in the behavior of CFT connection depends on the beam characteristics and column features.

Keywords: concrete filled tube, shear capacity, ductility, reversed cyclic loading, energy absorption

1. Introduction

Composite steel-concrete structures are used in civil engineering projects worldwide. In recent decades, concrete filled steel tube (CFT) structures have become accepted and used in buildings that they can provide the enhanced advantages of ductility associated with steel structures and concrete components (Roeder, 2000). The advantages of CFT columns over other steel-concrete composite structures called either mixed or hybrid systems include the fact that inside concrete prevents local buckling of steel tube wall and that the steel tube extends the ability of concrete spalling. Although the CFT can be an economical form of composite construction, their use has been limited due to the complexity of the beam-to-column connections and the limited construction experience. Previous studies on the structures showed that the analytical responses neglecting effect of connection configurations are rather different from experimental responses. Extensive experimental and analytical work have done to study the behavior of CFT connections under different loading conditions.

A wide range of beam-to-CFT column connections have been studied over the past several decades. Some type of connections transfer the load from the girders directly to the steel tube, while others transfer the load to both the concrete core and the steel tube. The connection types having girders welded to the steel tube are often suitable for simple connections (Dunberry *et al*., 1987; Shakir-Khalil and Mahmoud, 1995). However, for moment connections, these configurations impose high deformation demands on the steel tube, possibly causing fracture of the tube wall. This results in a deterioration of strength and stiffness. Thus, in some connection systems, it is common to distribute the girder force around the steel tube by means of internal and external diaphragm plates welded to the steel tube. Extensive experimental research on moment connections to circular concrete filled tube (CCFT) columns is available in literature. For connections to circular CFTs, Schneider and Alostaz (1998) found that the connection types having extended plates or deformed bars passing into the concrete core improved both strength and stiffness. Among their specimens, the one

Received September 19, 2016; accepted July 13, 2017;
published online March 31, 2018

*Corresponding author
E-mail: mehdi.ebadi1985@hotmail.com

with a continuous girder into the CFT column produced the most desirable cyclic response. Dunberry *et al*. (1987) investigated short square CFT columns that were loaded axially by means of shear tab connections coupled with direct axial compression. The authors proposed an equation for the cross section strength of CFT columns. Kamba *et al*. (1991) studied the panel zone behavior in moment-resisting CFT frames under monotonic loading. They proposed equations to estimate the elasto-plastic behavior of joint panels. Prion and McLellan (1992) conducted experimental studies of through-bolt connections between steel wide flange beams and concrete-filled hollow steel sections, and they compared their results to other types of CFT connections. Azizinamini *et al*. (1992) investigated both analytically and experimentally a through-beam connection detail. A behavioral model was developed and the force transfer mechanism of the through-beam connection detail was identified. Shakir-Khalil, and Al-Rawdan (1996) studied on simple beam-to-column connections of CFT members. A total six series of connections were tested, including both circular and square sections for the steel tubes (Shakir-Khalil, 1993a; 1993b; 1994a; 1994b; Kawano and Matsui, 1997) proposed new connection types to overcome the difficulty of external diaphragm details when placed near external walls if the diaphragm plates are large. These connections had the vertical stiffeners welded to the column face, substituting for the external diaphragm on one side. Schneider and Alostaz (1998) performed an experimental study that was conducted on steel girder to circular CFT beam-column exterior moment connections. Three-dimensional finite element analysis of various connection details was performed for monotonic flexural loading. They compared the performance of each detail and highlighted the differences and similarities observed in their inelastic cyclic responses. Three series of experiments on beam-to-column connections of HT and CFT columns were conducted (France *et al*., 1996; 1999a; 1999b; 1999c). The girders were connected to the steel tube wall. Both moment connections and simple connections were tested. The stiffness and strength properties of the connections were investigated and the effect of concrete filling on the connection performance was discussed. Cheng *et al*. (2000) tested beam-to-circular CFT column connections under cyclic loading. They investigated the effect of concrete infill and diameter to thickness of tube ratio on the seismic performance of the connections. Fujimoto *et al*., (2000) studied on half-scale internal and external CFT beam-to-column connections under reversed cyclic loading. The performance of the connections manufactured from high strength materials was the main focus of the research. An analytical study was carried out on panel zone behavior of steel beam-to-square CFT column connections (Fukumoto and Morita, 2000). They proposed a nonlinear stress-strain model to estimate the elasto-plastic response of the panel zone. An experimental study on beam-to-column connections of square CFT systems was presented by Ricles *et al*. (1997) and Peng *et al*. (2000). Full-scale cruciform specimens were tested under cyclic loading. Three types of connection details were utilized and their strength, stiffness, and ductility properties were investigated. Beutel *et al*. (2001) performed ten full scale connection tests. The connections tested utilized reinforcing bars which were welded to the flanges of the beams and embedded into the concrete. MacRae *et al*. (2004) developed a finite element model to study the transfer of vertical bracing forces through a beam-brace-column connection. Numerical and experimental studies of T-stub connections are presented by Yao *et al*. (2008). A numerical study in order to analyse the behavior of gusset plate CFT-to-bracing connections under an axial compressive force conducted by Hu *et al*. (2011). Failure of the connection was generally observed under the connection area. Ramadan *et al*. (2016) investigated the performance of different connection configurations between CCFT columns and gusset plates subjected to axial compression loadings. Vulcu *et al*. (2012) conducted an experimental program in order to characterise the behavior of moment resisting joints to CCFT columns in multi-storey frames. The specimens were tested under cyclic and monotonic loading.

Although, there has been numerous experimental and numerical work to study the behavior of CFTs under different loading conditions, research on connections to tubular CFT columns is limited. Therefore, a better understanding of the inelastic behavior of connections is needed to make CFT column connections as an alternative in composite construction. In this paper, the finite element analysis of CFT connections was conducted. The analysis incorporated geometric and material nonlinearities. The nonlinear behavior of concrete including crushing and cracking was included in the analysis. Numerical results were verified by comparison to published tests in literature. The verified model was used to investigate the effect of the geometric dimensions as well as connection configuration on the connection behavior including moment-drift curves, displacement ductility, ultimate load, and initial stiffness. In this research, the key objectives of the numerical parametric study are:

- Acquiring better understanding of key parameters (diameter of steel tube, wall thickness and length of beam and column) influencing on CFTs behavior under reversed cyclic loads.
- The effect of plate thickness to the beam connection steel tubular columns filled with concrete on the seismic behavior of connections is discussed.

2. Numerical Simulation

2.1. General

In this research, it is intended to conduct a rigorous and comprehensive investigation on seismic behavior of CFT connections. To achieve the accurate outcomes, structural

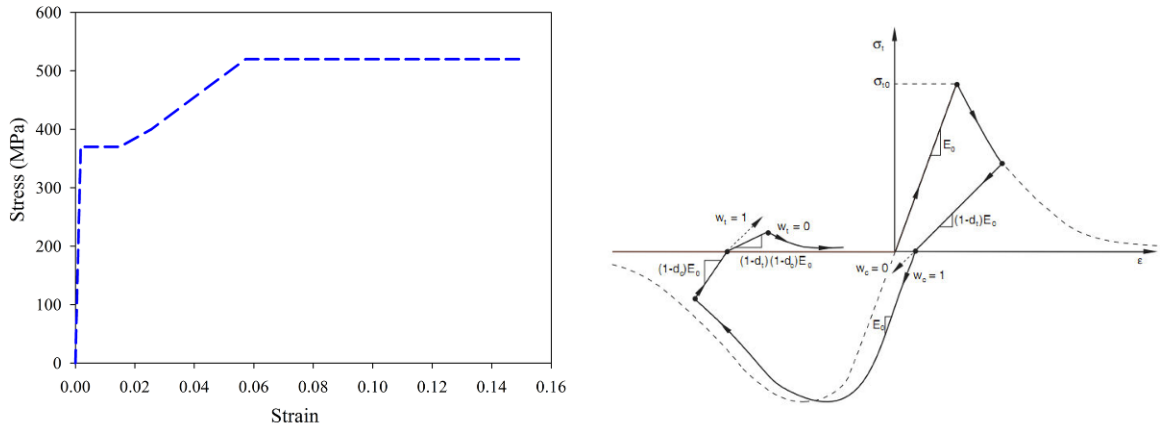

(a) Stress-strain curve of steel (b) Uniaxial load cycle for CDP model

Figure 1. Typical stress-strain curve of steel and normal-strength concrete.

models representing beam-column connections, will be utilized. The numerical analysis is carried out to investigate various factors affecting the seismic behavior, including thicknesses of steel tube wall, diameter of steel tube, cross-section area of beam and column and diameter to thickness ratio. The whole elements are modelled as an inelastic and an elastoplastic continuum materials. A comprehensive finite element model was generated for each connection type. These analytical models were generated to investigate the influence of various detail components on the connection seismic behavior. ABAQUS v6.13.1 was used to analyse the 3-D nonlinear finite element models of the proposed details.

2.2. Material constitutive models

The reliability of these finite element analyses depended, among other factors, on how accurately the material properties were mathematically modelled. Each analytical model had three basic types of elements: concrete, steel, and the interface between the steel and the concrete. The uniaxial behavior of the steel tube can be simulated by an elastic-perfectly plastic model with an associated flow rule. When the steel tube is subjected to multiple stresses, a Von Mises yield criterion, F, is employed to define the elastic limit, which is written as:

$$F = \sqrt{3J_2} = \frac{1}{\sqrt{2}}\sqrt{\left(\sigma_1 - \sigma_2\right)^2 + \left(\sigma_2 - \sigma_3\right)^2 + \left(\sigma_3 - \sigma_1\right)^2} = \sigma_y \quad (1)$$

where J_2 is the second stress invariant of the stress deviator tensor and σ_1, σ_2, and σ_3 are the principal stresses. It was presumed that the steel behavior under tension was identical to that under compression. The steel is presumed to behave as an elastic-plastic material with strain hardening after yield strength. The von Mises yield surface and associated plastic flow is considered for steel material. Steel properties in ABAQUS comprised of a young's modulus of steel (E_s), a poisson's ratio (n_s) and a yield strength. The young's modulus, poisson's ratio, yield strength (f_y), and ultimate strength (f_u) of steel were presumed to be 200 GPa, 0.3, 370, and 520 MPa, respectively (Fig. 1(a)).

For a concrete-filled steel tube, confinement of the concrete core was not fully understood. ABAQUS software was selected for all finite element computations, because of its available 3D inelastic concrete material model. When the principal stresses were predominantly compressive, the concrete was modelled by an elastic-plastic theory using a simplified yield surface. Cracking was assumed to be the most important aspect of the material behavior. Cracking was assumed to occur when the stresses reached the failure surface. Figure 1(b) shows the uniaxial behavior of concrete in this model while subjected to cyclic loads. For tension in the concrete material, the behavior was linear up to its tensile strength. This tensile strength was assumed to be 10% of the uniaxial compressive strength. Since cracks in plain concrete cannot transfer tensile stresses, the post tensile strength stiffness was quite steep. Shear retention was used to describe the reduction in the shear modulus associated with the concrete cracking. It was assumed that the shear response was not affected by cracking. This assumption was reasonable, and in many cases, the overall response was not strongly dependent on the amount of shear retention.

A Concrete Damaged Plasticity (CDP) model in ABAQUS is used to simulate the behavior of concrete encased in steel tube. This model is a continuum plasticity-based damage model and assumes tensile cracking and compressive crushing to be the two main failure mechanisms of the concrete material. The CDP model expresses behavior in terms of effective stress and hardening variables, such that:

$$\sigma = \left(1 - d\right) D_0^{el} : \left(\varepsilon - \varepsilon^{pl}\right) = D^{el} : \left(\varepsilon - \varepsilon^{pl}\right) \quad (2)$$

$$\bar{\sigma} = D_0^{el} : \left(\varepsilon - \varepsilon^{pl}\right) \in \left\{\bar{\sigma} \middle| F\left(\bar{\sigma}, \tilde{\varepsilon}^{pl}\right) \le 0\right\} \quad (3)$$

$$\tilde{\varepsilon}^{pl} = h\left(\bar{\sigma}, \tilde{\varepsilon}^{pl}\right).\dot{\varepsilon}^{pl} \tag{4}$$

$$\dot{\varepsilon}^{pl} = \dot{\lambda}\frac{\partial G\left(\bar{\sigma}\right)}{\partial \bar{\sigma}} \tag{5}$$

where σ is the Cauchy stress, $\bar{\sigma}$ is the effective stress, D_0^{el} is the initial undamaged elastic stiffness, d is a scalar stiffness degradation variable, (which can vary between zero for undamaged material to one for fully damaged material), ε and ε^{pl} are total strain and plastic strain, $(\bar{\sigma}, \tilde{\varepsilon}^{pl}) \le 0$ is the yield function, $\tilde{\varepsilon}^{pl}$ is the hardening variable which is also referred to as the equivalent plastic strain, h defines the evolution of hardening variables, and G is a flow potential which governs the plastic flow.

Many researchers (Mander *et al*., 1988; Susantha *et al*., 2001; Sakino *et al*., 2004) have shown that concrete confined by a circular steel tube can exhibit increased strength and ductility. These effects can be considered in the CDP model by modifying the stress-strain expression (f_c-ε) of concrete in uniaxial compression defined by Popovics (1973) and later modified by Mander *et al*. (1988), to become:

$$f_c = f_{cc}'\frac{xr}{r-1+x^r} \tag{6}$$

$$x = \frac{\varepsilon}{\varepsilon_{cc}} \tag{7}$$

$$r = \frac{E_c}{\left(E_c - f_{cc}'/\varepsilon_{cc}\right)} \tag{8}$$

$$\varepsilon_{cc} = \varepsilon_c\left[1+5\left(\frac{f_{cc}'}{f_c'}-1\right)\right], f_{cc}' = f' + mf_{rp} \tag{9}$$

where f_c' and ε_c are the maximum strength and corresponding strain value for unconfined concrete, f_{cc}' and ε_{cc} refer to the same parameters for confined concrete, and E_c stands for the modulus of elasticity of concrete. f_{rp} is the maximum radial pressure on concrete and m is an empirical coefficient (in the range of 4-6). It should be mentioned that this expression works for the whole uniaxial curve (before and after peak), but it is also common to model the post-peak behavior as a linear descending branch, starting from the peak point and ending at the point with the coordinates $(\varepsilon_{cu}, \alpha f_{cc})$, after which the material is taken to have a constant stress αf_{cc}' referred to as the residual stress. Since it is difficult to come up with a mathematical expression for the parameter ε_{cu}, it is considered here as having a constant value of 0.025 in all cases, which can be considered acceptable based on the analyses done by Usami *et al*. (2001) The α multiplier is determined by calculating the softening slope (Z), from the peak point; for concrete confined having circular sections, and they have proposed the following equations to calculate Z, based on calibration with experimental data:

$$Z = 1.0\times10^5 R_t\frac{f_c'}{f_y} - 6000$$
$$R_t = \sqrt{3\left(1-\nu^2\right)}\frac{f_y}{E_s}\frac{D}{2t} \tag{10}$$

where f_y is the yield stress of steel and in which D and t are the outer steel tube's diameter and thickness respectively.

The compressional and tensile damage parameters are considered as a linear function of inelastic strains. For the structural concrete utilised in analysis, specified compressive strength (f_c') and mass density (ρ_c) are assumed to be 35 MPa and 2350 kg/m^3, respectively. The modulus of elasticity of concrete (E_c) is calculated to be 27805 MPa according to ACI code. The average strain at peak stress of the normal strength concrete is 2225 $\mu\varepsilon$, which is a typical value. The poisson's ratio of the normal-strength concrete (0.13) is typical of accepted values (0.11 to 0.21) for normal-strength concrete according to the ACI report 363R-92.

2.3. Steel-concrete interface

Contact between steel and concrete must be modeled in concrete filled steel tubes. The models used for this purpose must be able to account for the forces to be transferred at the interface when these surfaces are in contact, while allowing the two materials to separate from each other if needed. Two situations are possible for these surfaces through the whole loading process, including the times that they are actually in contact and times they are separated from each other because of the deformations of the tubes and concrete core. For modelling of CFT members in buildings, a surface-based interaction is used to represent the contact between the steel tube and the concrete. The normal direction of the two surfaces is hard contact that they cannot intrude together and the tangent contact is simulated by the coulomb friction model (Chang *et al*., 2012; 2013). According to the existing studies (Chang *et al*., 2012; 2013; Ellobody and Young, 2006) the coefficient of friction used for CFT columns under axial compression ranged from 0.3 to 0.5. Both tangential and normal contacts were employed to define contact properties between the steel and the concrete core. As the composite column is not sensitive for the value of friction coefficient in steel and concrete, the friction contact among the parts was defined using coulomb friction with friction coefficient of 0.4 which agrees to the test results and finite element model.

Table 1. Loading protocol history

N*	3	3	3	2	2	2	2	2	2	2	2	2	2	2	2
Drift (%)	0.375	0.5	0.75	1	1.5	2	3	4	5	6	7	8	10	11	13

*N= Number of cycles

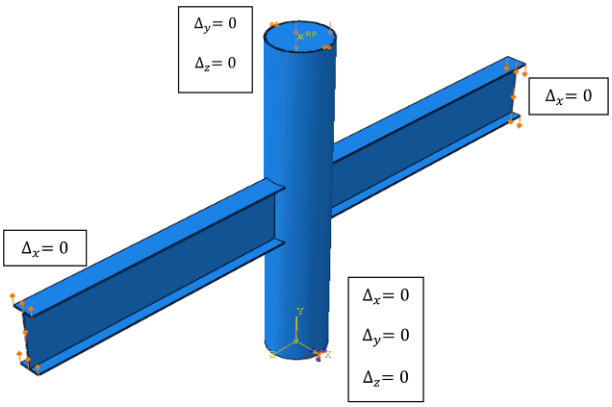

Figure 2. Boundary conditions and loading.

2.4. Finite elements

Twenty-node brick elements (C3D20 of ABAQUS library elements) with three translational degrees of freedom at each node were used to model the concrete core. Eight-node shell elements (S8R5) with five degrees of freedom at each node were used to model the steel tube and the girders. All the elements incorporated material and geometric nonlinearities in their formulation. Nodal displacement compatibility was enforced between the solid and shell elements. However, no rotation compatibility was enforced between the two element types. Convergence of the numerical solution was checked by varying the number of elements and nodes in each model. Based on these convergence studies, the type of finite elements and the size of the finite element mesh were selected.

2.5. Boundary conditions and load application

The boundary conditions applied to the model are pinned-pinned at both column ends while one end is allowed to have horizontal displacement as in the test setup. Axial load was applied as a constant pressure on the end and the lateral load was directly applied to the beam edge (Fig. 2). Loading history in these tests consisted of 15 cycles. It started with 0.375% drift ratio. Each amplitude was repeated two times (except of first three cycles) to evaluate the strength and stiffness degradation. The cycle amplitudes increased up to 13% drift ratio, as shown in Table 1. The drift ratio was evaluated by dividing the column lateral displacement to column height. The loading pattern used in this study is the combination of loading patterns of ATC-24, AISC 341-10, ACI 374.1-05.

2.6. Comparison of numerical simulation with experimental results

In this section, to assess the capability of the developed numerical model in simulating the CFT connection, the results of the conducted revresed cyclic tests (Elremaily and Azizinamini, 2002) are employed to verify and calibrate the developed numerical model in ABAQUS. In this paper, six circular CFT beam-column specimens

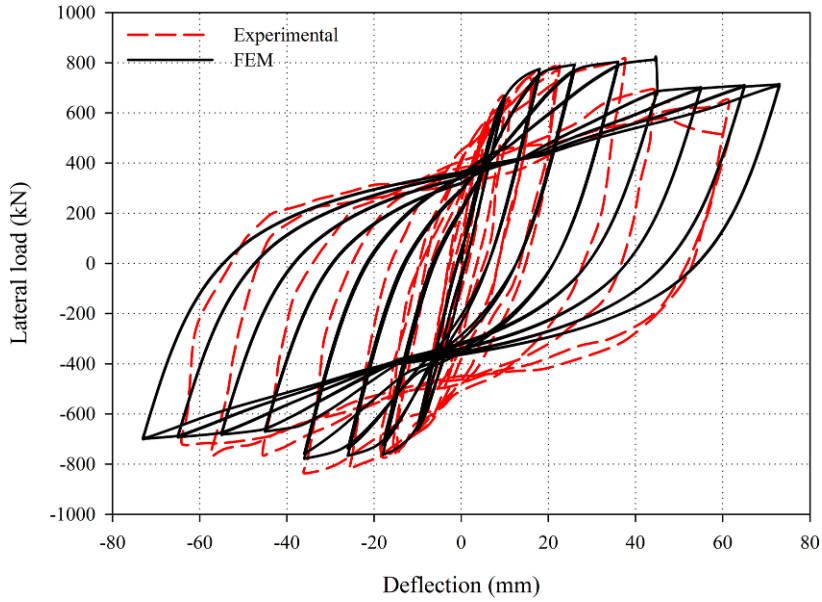

Figure 3. The lateral load-displacement curves of experimental and numerical simulation.

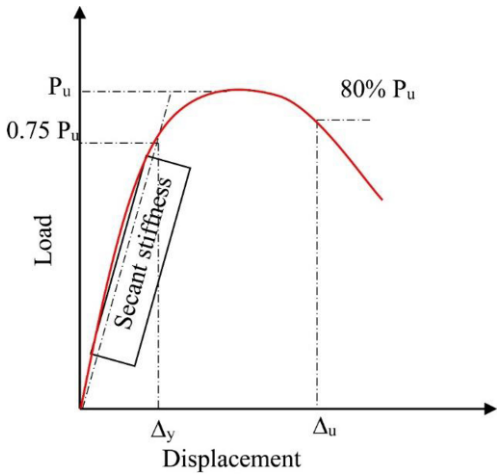

Figure 4. Definitions of yield displacement and maximum displacement.

were selected to be approximately two-thirds scale of columns for a typical prototype building. The diameter of the specimen was 325 mm with a *D/t* ratio of 51. The column was subjected to constant axial load between 0.2 and 0.4 of the column squash load (P_0). P_0 calculated as the summation of the ultimate axial capacities of both the steel and concrete. This ratio was selected 0.4. Wall thickness and the target concrete compressive strength were 6.4 mm and 40 MPa, respectively. The average yield stress of the steel tubes was found to be 372 MPa. The relationship between lateral load and deflection is shown in Fig. 3. Comparison of the numerical predictions and the experimental data shows a good agreement confirming the reliability of the numerical model. It can be concluded that the FE model and material constitutive adopted in this paper are reasonable. The load-deflection curves show full hysteretic loops without a significant drop in the strength. The results indicated that the transformed stiffness was a good approximation for initial stiffness. Table 2 presents the summary of the test and FEM results. As shown in Fig. 4, the yield displacement Δ_y was defined using the secant stiffness connecting the origin and 75% of the peak load (Mander *et al*., 1988). Maximum displacement Δ_u was defined as the postpeak displacement corresponding to 80% of the peak strength (Mander *et al*., 1988).

3. Parametric Study

The parametric study is conducted using the model on 84 circular CFT column-steel beam connections to investigate the effect of three main parameters on steel beam-CFT column performances. The load carrying capacity, ductility, and energy absorption of specimens are explored. The first examined parameter is the thickness of steel tube wall. Two thickness values equal to 6 and 12 mm are considered. The second parameter is the depth of beam that is taken equal to 450, 700 and 800 mm. The final parameter is the thickness of flange of beam that is taken equal to 10 and 20 mm. The web thickness and width of flange of beam are constant (7.6 and 250 mm, respectively) in all specimens. Connection plates comprised of continuity plate and flange plates that have the same width (400 mm). It should be noted that all analysed steel beam-CFT column connections have circular cross-section column with length to diameter ratio (*L/D*) equals to 6. Length of

Table 2. Summary of test and FEM results

	Maximum strength P_u (kN)	Yield displacement Δ_y (mm)	Maximum displacement Δ_u (mm)	Ductility μ (=Δ_u/Δ_y)	Yield stiffness k_y (=P_u/Δ_y) (kN/mm)
Experimental	805.31	9.25	43.65	4.72	87.06
FEM	812.95	9.13	45.18	4.95	89.04

Table 3. Specimen features

Group Number	Specimen Number	Thickness of flange (mm)	Depth of beam (mm)	Thickness of steel tube column (mm)
1	1-7	10	450	6
2	8-14	10	700	6
3	15-21	10	800	6
4	22-28	20	450	6
5	29-35	20	700	6
6	36-42	20	800	6
7	43-49	10	450	12
8	50-56	10	700	12
9	57-63	10	800	12
10	64-70	20	450	12
11	71-77	20	700	12
12	78-84	20	800	12

column and beam are taken equal to 2400 mm and 1850 mm. The specimens were named according to the Eq. (11).

$$n.\ fm_t d_t,\ C_d T_t,\ B_h T_t \tag{11}$$

n = Specimen number of
f = Specimen with concrete
m_t = Continuity plate with considered thickness
d_t = Presense of flange plates
$C_d T_t$ = Diameter and thickness of column
$B_h T_t$ = Depth of beam and thickness of flange

In some specimens, f letter replaced by O letter that represents lack of presence of concrete. All plates are circular shape and their thickness change with flange thicknesses. Table 3 describes the specimen features.

4. Results and Discussions

4.1. Lateral load-displacement relationship

In this section, we try to comprehensively compare the load-bearing capacity using specimens obtained from the specimen analysis. Then, the connection stiffness, flexural capacity, ductility and the rate of energy absorption were taken into consideration. Stiffness, strength and ductility are three basic needs of a seismic design forming the capacity of a structure, which is discussed in detail.

Based on the Fig. 5(a) in group 1, the most bearing capacity pertained to the steel connection specimen filled with concrete with flange plates and continuity plate. The bare steel connection with continuity plate accounted for the lowest bearing capacity. As observed in group 2 (Fig. 5b), the flexural moment of connections increased compared to the group 1. Specimen 20 had a lateral buckling in the beam and tolerated lower strength (Fig. 5(c)). A comparison between Figs. 5(a-c) revealed that most of the flexural stiffness and bearing capacity concerned with the simultaneous use of continuity and flange plates with concrete. However, it was observed that an increase in the depth of the beam increased its lateral buckling and reduced its bearing capacity. Figure 5(c) indicated that load-bearing capacity in the specimen 21 was 5% more than the specimen 20. An increase in the beam flange thickness from 10 to 20 mm resulted in enhancing the load-bearing capacity in the similar specimens with flange thickness 10 mm. Based on the Fig. 5(d), as expected, the specimen No. 27 accounted for the maximum bearing capacity. The use of flange plates increased the lateral bearing capacity of the specimen compared to the continuity plates. The comparison of the specimens 24 and 26 with no concrete revealed 30% difference between their maximum bearing capacities. The increase in the beam flange thickness declined the lateral bearing capacity of the specimen more than the increase in the beam depth, which was due to early lateral buckling. That is why the bearing capacity enhanced, compared to the similar specimens, in specimens without concrete and continuity and flange plates (Fig. 5(e) and 5(f)).

As observed in Figs. 6(a) and 6(b), the maximum and minimum capacities were related to the specimens with flange and continuity plates, and with and without concrete, respectively. The continuity plates had an insignificant effect on increasing the lateral load capacity of the specimens. Figure 6(c) indicates that increasing the beam depth caused lateral torsional buckling in the beam. Increasing the thickness of the steel column from 6 to 12 mm enhanced the bearing capacities, compared to the similar specimens. Other specimens in Fig. 6(d-f) showed similar behaviors.

The stress-strain behavior of steel and concrete in CFT columns was due to the interaction between multi-variate and multi-axis steel and concrete which resulted in an increase in the strength and ductility. The research compared the two specimens 1 and 22 to study the stresses and strains caused in the steel and concrete. Figure 7(a) and 7(b) illustrate von Mises stress in steel, Fig. 8(a) and 8(b) show plastic strains, and Fig. 9(a) and 9(b) illustrate the tension in the tensile and compressive parts of concrete.

As shown in Fig. 7, the panel zone dramatically affected the beam flange thickness in the specimen 22 regarding the energy dissipation in the connection and the connection behavior in severe earthquakes. Because a weak panel zone causes much deformation resulting in brittle fracture connection even with a fully rigid connection (connection strength higher than the beam leading to a fracture of area other than the connection area) which happened when the purpose of designing this system was to achieve sufficient ductility and prevent brittle fracture. Transferring moment between the beams and columns led to a complex condition of stress and strain at the connection and in the connection spot which created many normal stresses on the beam flanges as well as a high shear stress in the connection part.

Although the stress concentration coefficient decreased due to the redistribution of excess stress on the yield stress on non-yield areas, and the stress field approached the uniformity, the strain concentration factor significantly increased due to its rapid rate of growth because of yielding of materials. Connection fractures of CFTs started from the joints of stress concentration. However, the structure is placed under cyclic loading during an earthquake, which the fracture occurred in high strain intensity (Fig. 8).

4.2. Influence of flange thickness of steel beam on ductility

The expression of displacement ductility coefficient (μ) of CFT component is shown in Fig. 4. Where: The Δ_y represents the displacement corresponding to the yield strength, namely yield displacement; The Δ_u represents the ultimate displacement.

It is widely recognized that load-displacement curve is

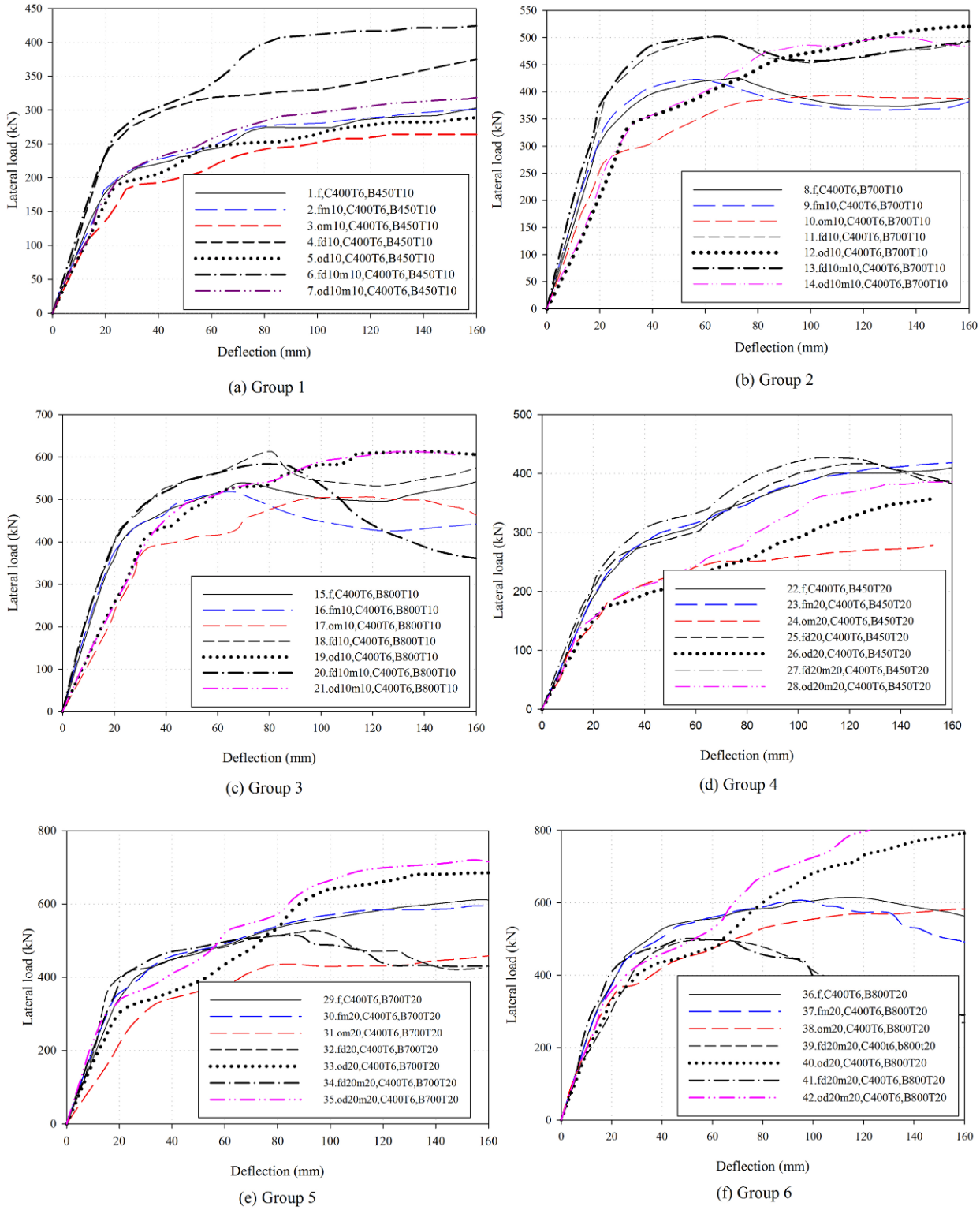

Figure 5. Lateral load-displacement relationships of different groups with the wall thickness value equal to 6 mm.

one of the most important profiles to show the performance of materials. As shown in the load-displacement curve for the CFT specimens, there is no the obvious yield point. Therefore, the method to determine the yield displacement Δ_y is to draw between the tangent line of the P-Δ skeleton line at the origin point and the tangent line at the peak point. The displacement of the intersection point is the yield displacement. For the ultimate displacement, its value is equivalent to the displacement corresponding to the 85% bearing strength in the decline period.

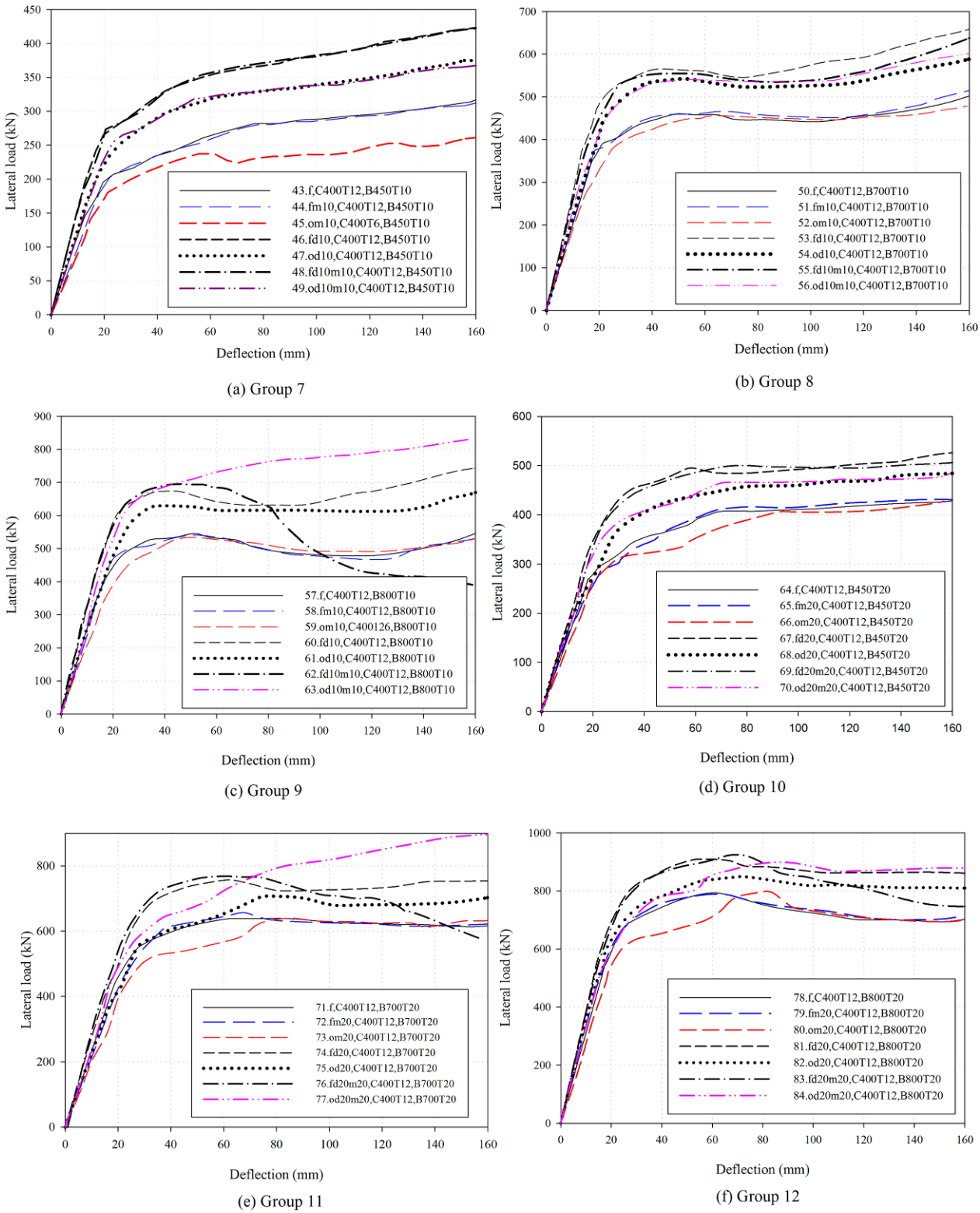

Figure 6. Lateral load-displacement relationships of different groups with the wall thickness value equal to 12 mm.

Table 4 indicates the elastic stiffness and ductility factor of all the specimens. Increasing the beam flange thickness in the similar specimen could decrease the ductility. The ductility reduction was observed in cases with and without concrete. Increasing the beam flange thickness from 10 to 20 mm, reduced ductility in the specimen 5 by 4.7% compared to specimen 26. The ductility in other specimens such as specimen 49 reduced by 4.2%,

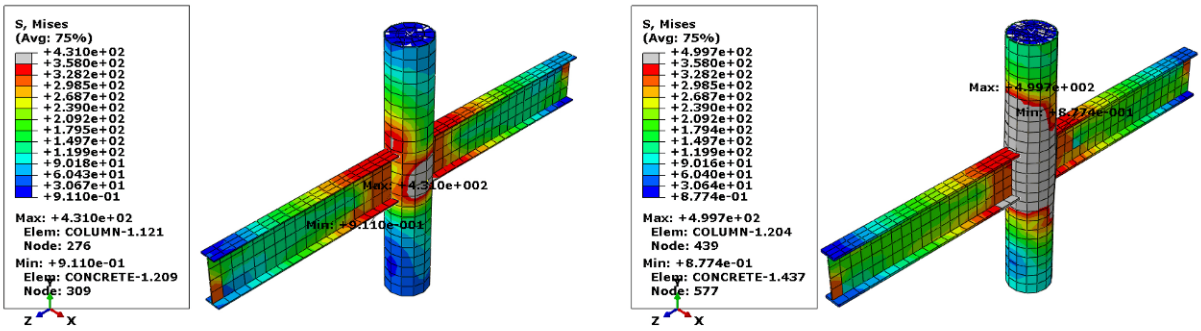

(a) Specimen 1 (a) Specimen 22

Figure 7. Stress distribution in steel components of specimens.

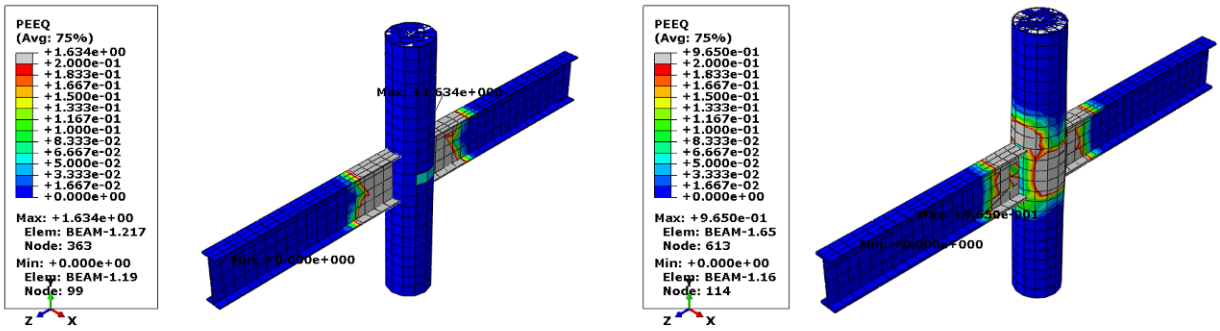

(a) Specimen 1 (a) Specimen 22

Figure 8. Plastic strain contour in steel components of specimens.

compared to the specimen 70%. Specimen 42 accounted for the highest drop in ductility among the steel column categories with a thickness of 6 mm which was 26%. This reduction for the groups of steel column with wall thickness 12 mm equaled to 40% in the specimen 80. The reduction in the ductility in the specimens without concrete was more than those filled with concrete. Moreover, an increase in the beam depth failed to indicate a regular changing trend in the ductility of specimens. However, only in specimens with a steel column and wall thickness 12 mm and beam flange thickness 20 mm, the reduced ductility was inversely related to the beam depth. In all cases, the use of continuity plates increased ductility more than the similar specimens with flange plates. The specimen 16 accounted for the most ductility factor with a beam depth 800 mm, and value 5.62. The lowest ductility related to the specimens of group 12. In addition, the ductility decreased by increasing the wall thickness of the steel columns and with the stability of other parameters in the same specimen. However, in the specimen without concrete, by increasing the wall thickness of the steel columns and with the flange and continuity plates, the ductility increased by 27 and 17% in specimens 63 and 84.

Table 5 compares group 1 and 4, in terms of ductility, displacement and ultimate load. In CFTs, in all specimens, the most optimal ductility situation pertained to the beam depth 700 mm and the stiffness in beam depth of 700 mm increased by 14%, compared to other connections. Increase in the beam flange thickness in the CFT structures decreased connection ductility by 12%, and such decrease in the hollow steel column connections reached 26%. Furthere, this comparison showed more ductility of CFT connections, compared to hollow steel column connections.

4.3. Moment-drift relationship

Comparison of moment rotation curves (Fig. 9) reveals that inelastic deformations in plastic hinge regionof beam are significantly larger than the other regions. In these connections shear panels have behaved linearly. Also, nonlinear behavior is developed only when large amounts of moments are applied to the connection. Beam plastic hinge region has already undergone large inelastic deformations. Moment calculated from length of beam multiple displacement on beam tip.

Due to a high number of graphs, the researcher only compared the two groups 1 and 4 in terms of flexural capacity in Fig. 9. In all specimens, while other conditions remained constant, an increase in the thickness of the beam flange resulted in boosting the flexural moment connection. However, the trend was reversed in some specimens with the lateral torsional buckling of beam. The best flexural behavior pertained to the specimen with a beam depth of 700 mm. In this case, the difference

Table 4. Stiffness and ductility coefficient values for all specimens

Specimen	Stiffness (kN/m)	Ductility coefficient	Specimen	Stiffness (kN/m)	Ductility coefficient	Specimen	Stiffness (kN/m)	Ductility coefficient
1	9134	3.65	30	19047	3.13	59	24042	4.66
2	9453	3.67	31	14552	3.53	60	35478	4.04
3	7358	3.98	32	22537	3.35	61	31374	3.70
4	12725	2.91	33	15899	2.07	62	37150	3.36
5	8004	3.18	34	24395	3.30	63	31817	2.85
6	12995	3.79	35	19176	2.19	64	14370	3.97
7	9352	3.46	36	24988	3.73	65	14620	3.89
8	17069	3.70	37	25993	5.34	66	12342	4.01
9	18600	3.75	38	19264	2.29	67	17449	3.98
10	13480	3.91	39	26179	4.43	68	15680	3.18
11	20770	3.67	40	19318	2.18	69	17731	4.24
12	11256	2.25	41	27632	4.24	70	15812	2.61
13	21967	3.84	42	19743	2.01	71	26488	3.94
14	11481	2.25	43	10875	4.27	72	26598	3.85
15	22448	4.29	44	11375	4.06	73	22953	3.18
16	23589	5.62	45	9703	4.25	74	28947	3.57
17	12154	2.73	46	15680	4.20	75	26855	3.11
18	24894	4.74	47	11451	3.45	76	29745	3.22
19	12954	2.88	48	16752	4.31	77	28197	3.06
20	25669	4.61	49	12070	2.72	78	32418	2.67
21	13227	2.72	50	22173	4.20	79	33217	2.63
22	10926	3.50	51	22546	4.13	80	27900	2.76
23	11056	3.41	52	19480	4.05	81	35618	2.79
24	8848	3.31	53	27069	3.93	82	32518	2.75
25	15999	2.88	54	22638	3.85	83	38294	2.72
26	8975	3.03	55	27918	3.43	84	34613	2.63
27	13311	2.82	56	24598	3.74			
28	9598	3.06	57	27906	4.23			
29	18423	3.20	58	28295	4.16			

Table 5. Effect of flange thickness on stiffness and ductility (comparison between group 1 and 4)

Percentage of ductitlity %	Ductility coefficient $\mu=\Delta_u/\Delta_y$	Ultimate load (kN)	Yield load (kN)	Ultimate displacement (m) Δ_u	Yield displacement (m) Δ_y	Stiffness of connection k	Name of specimen	Row
4.2	3.65	272	221	0.0885	0.02424	9134	7	1
0	3.50	386	302	0.099	0.02770	10926	28	
7.6	3.67	276	225	0.0876	0.02384	9453	8	2
0	3.41	395	304	0.0940	0.02755	11056	29	
6.9	3.98	247	208	0.0948	0.02853	7358	9	3
0	3.31	275	209	0.099	0.02987	8848	30	
11.1	2.91	360	230	0.0766	0.02598	12725	10	4
0	2.88	470	354	0.070	0.02430	15999	31	
4.9	3.18	345	222	0.0881	0.02768	8004	11	5
0	3.03	409	287	0.086	0.02839	8975	32	
21.2	3.79	395	264	0.077	0.02030	12995	12	6
0	2.82	499	376	0.067	0.02155	13311	33	
13	3.46	358	234	0.085	0.02451	9352	13	7
0	3.06	416	298	0.073	0.02384	9598	34	

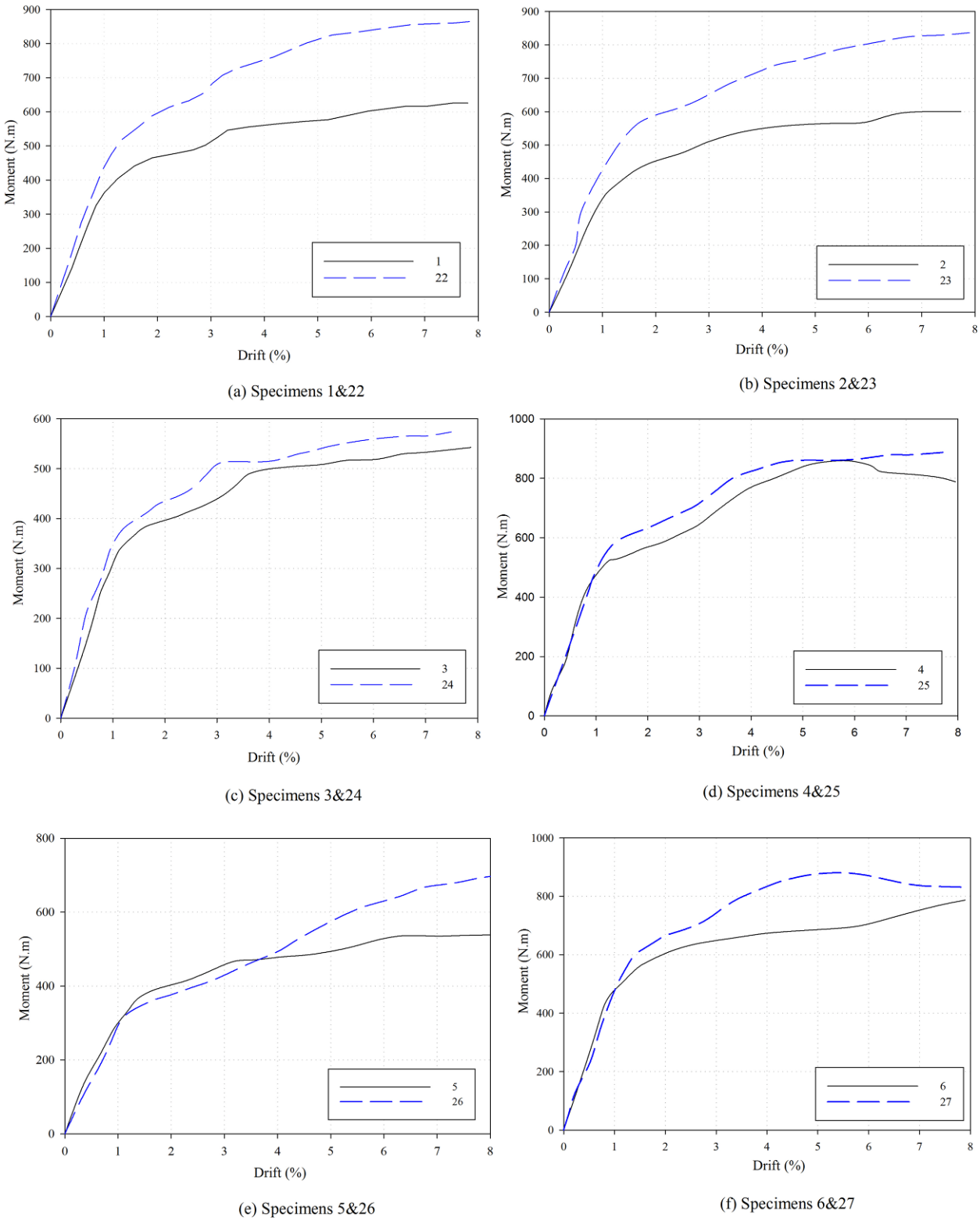

(a) Specimens 1&22

(b) Specimens 2&23

(c) Specimens 3&24

(d) Specimens 4&25

(e) Specimens 5&26

(f) Specimens 6&27

Figure 9. Comparison of moment-drift curve between specimens of group 1 and 4.

between the flexural capacity among the specimens with higher flange thickness to those with lower flange thickness was approximately 5%.

4.4. Energy absorption in connections

To avoid ambiguity of interpretation, the energy dissipation was determined to a point equal to 95% of M_P on the

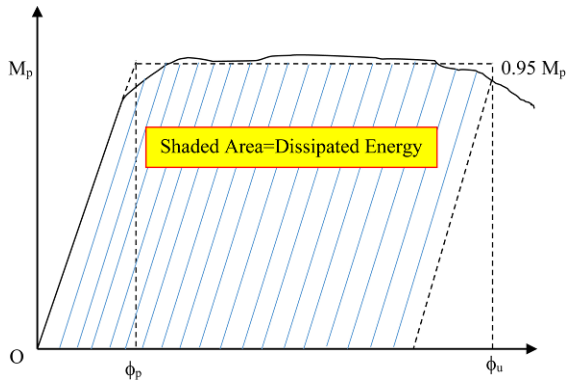

Figure 10. Absorbed energy under uniform moment.

unloading part of the curve (Fig. 10). The 95% cutoff is entirely arbitrary and serves only to assure uniform interpretation of the results.

In CFT connections with 400 mm diameter of column and 450 mm beam depth, the energy absorbed by the connections due to change in the thickness was 32% higher than hollow steel specimens, indicating that the proper performance level of CFTs dissipated more energy. This value for the similar specimens was reduced to 12% by varying the beam depth from 450 to 700 mm. In general, in specimens with low beam depth, when a change takes place in the flange thickness, the amount of energy absorption of CFT connections exceeds those with hollow steel columns increasing by 33%. Increasing the beam depth could decrease the energy absorption of concrete filled steel column with flange plates by 30% than the same model with lower flange thickness.

5. Concluding Remarks

In this paper, the finite element ABAQUS software has been used for analysing the connection effect on CFTs. For verification of modelling, an experimental sample that its results were available has been modelled and compared with experimental results. Non-linear static analysis has been done on sample for investigating the behavior of CFT connections, then according to ATC-24 loading model, a nonlinear static analysis has been done and hysteresis curves have been obtained. The parameters of resistance such as ductility coefficient, ultimate strength, energy dissipation and stiffness have been obtained from hysteresis curves. Based on the results, some conclusions can be obtained as follow.

(1) The most optimal ductility in the connections related to the beam with a depth 700 mm, the ductility of which was increased by 14% than other CFT connections.

(2) An increase in the flange thickness in specimens could reduce connection ductility by 18%, which touched 26% in the hollow steel column connections. Based on the comparison, the ductility of CFT connections was substantially higher than hollow steel column connections.

(3) In specimens with low beam height, varying the flange thickness significantly increased the rate of energy absorption of CFT connections than connections with hollow steel columns.

(4) In those cases where the concrete filled steel columns were along with the flange and continuity plates, and the height of the beam was high, the beam lost its bearing capacity for lateral buckling and the specimen was damaged due to the high column stiffness and constant beam web thickness.

(5) The flange plates could further enhance the lateral load capacity, compared to the continuity plates in the specimen. The increase in the flange thickness of the beam reduced the lateral bearing capacity more than the increase in the beam depth, due to the early lateral buckling. Therefore, specimens without concrete, continuity and flange plates have increased the bearing capacity, compared to the similar specimens.

(6) The highest and lowest capacity was related to the continuity and flange plates with and without concrete, respectively. The presence of the continuity plates had an insignificant effect in increasing the lateral bearing capacity of the specimens. Increasing the beam depth led to the lateral torsional buckling in the beam. By increasing the wall thickness of steel columns from 6 to 12 mm, the bearing capacity of the specimen could increase, compared to similar specimens.

References

ABAQUS Standard User's Manual The Abaqus Software is a product of Dassault Systèmes Simulia Corp., Providence, RI, USA Dassault Systèmes, Version 6.13.1, USA; 2013.

ACI. (1997). ACI 363R-92, State-of-the-art report on high-strength concrete (reapproved in 1997). American Concrete Institute, Farmington Hills, MI.

ACI 374.1-05 (Reapproved 2014). Acceptance criteria for moment frames based on structural testing and commentary, Reported by ACI Committee 374, 2005.

AISC 341-10, (2010). Seismic Provisions for Structural Steel Buildings, American Institute of Steel Construction, Chicago, IL.

ATC, (1992). Guidelines for Cyclic Seismic Testing of Components of Steel Structures, ATC-24, Applied Technology Council, Redwood City, CA.

Azizinamini, A., Prakash, B., Prishtina, B., and Salmon, D. C. (1992). "Through Connection Detail for Composite Columns in Highrise Buildings", *Proceedings of the SSRC Annual, Technical Meeting,* Pittsburgh, Pennsylvania, Structural Stability Research Council, Bethlehem, Pennsylvania, pp. 225-236.

Beutel, J., Thambiratnam, P. D., and Perera, N. (2001). "Monotonic Behavior of Composite Column to Beam Connections", *Engineering Structures*, 23(9), pp. 1152-1161.

Chang, X., Wei, Y. Y., Yun, Y. C. (2012). "Analysis of steel-reinforced concrete-filled steel tubular (SRCFST) columns under cyclic loading", *Construction and*

Building Materials, 28(1), pp. 88-95.

Chang, X., Ru, Z. L., Zhou, W., and Zhang, Y. B. (2013). "Study on concrete-filled stainless stee-carbon steel tubular (CFSCT) stub columns under compression", *Thin-Walled Structures*, 63, pp. 125-133.

Cheng, C., Hwang, P., and Chung, L. (2000). "Connection Behaviors of Steel Beam to Concrete-Filled Circular Steel Tubes", Composite and Hybrid Structures, *Proceedings of the Sixth ASCCS International Conference on Steel-Concrete Composite Structures*, Xiao, Y. and Mahin, S. A. (eds.), Los Angeles, California, Association for International Cooperation and Research in Steel-Concrete Composite Structures, Los Angeles, California, pp. 581-589.

Dunberry, E., LeBlanc, D., and Redwood, R. G. (1987). "Cross-Section Strength of Concrete-Filled HSS Columns at Simple Beam Connections", *Canadian Journal of Civil Engineering*, 14(3), pp. 408-417.

Ellobody, E., and Young, B. (2006). "Design and behavior of concrete-filled cold-formed stainless steel tube columns", *Engineering Structures*, 28(5), 716-728.

Elremaily, A. and Azizinamini, A. (2002). "Behavior and strength of circular concrete-filled tube columns", *Journal of Constructional Steel Research*, 58(12), pp. 1567-1591.

France, J. E., Davison, J. B., and Kirby, P. A. (1996). "Experimental Testing of Flowdrill Connectors with Concrete-Filled SHS Columns", Tubular Structures VII, *Proceedings of the Seventh International Symposium on Tubular Structures*, Farkas J. and Jarmai, K. (eds.), University of Miskolc, Hungary, pp. 333-340.

France, J. E., Davison, J. B., and Kirby, P. A. (1999a). "Strength and Rotational Response of Moment Connections to Tubular Columns Using Flowdrill Connectors", *Journal of Constructional Steel Research*, 50, pp. 1-14.

France, J. E., Davison, J. B., and Kirby, P. A. (1999b). "Strength and Rotational Stiffness of Simple Connections to Tubular Columns Using Flowdrill Connectors", *Journal of Constructional Steel Research*, 50, pp. 15-34.

France, J. E., Davison, J. B., and Kirby, P. A. (1999c). "Moment Capacity and Rotational Stiffness of Endplate Connections to Concrete-filled Tubular Columns with Flowdrilled Connectors." *Journal of Constructional Steel Research*, 50, pp. 35-48.

Fujimoto, T., Inai, E., Tokinoya, H., Kai, M., Mori, K., Mori, O., and Nishiyama, I. (2000). "Behavior of Beam-To-Column Connection of CFT Column System Under Seismic Force", Composite and Hybrid Structures, *Proceedings of the Sixth ASCCS International Conference on Steel-Concrete Composite Structures,* Xiao, Y. and Mahin, S. A. (eds.), Los Angeles, California, March 22-24, 2000, Association for International Cooperation and Research in Steel-Concrete Composite Structures, Los Angeles, California, pp. 557-564.

Fukumoto, T. and Morita K. (2000). "Elasto Plastic Behavior of Steel Beam to Square Concrete Filled Steel Tube(CFT) Column Connections." Composite and Hybrid Structures, *Proceedings of the Sixth ASCCS International Conference on Steel-Concrete Composite Structures*, Xiao, Y. and Mahin, S. A. (eds.), Los Angeles, California, March 22-24, 2000, Association for International Cooperation and Research in Steel-Concrete Composite Structures, Los Angeles, California, pp. 565-572.

Hu H. T., Chen C. W., and Huang M. Y., (2011), "Nonlinear finite element analysis of CFT-to-bracing connections subjected to axial compressive forces", *J. Eng. Struct.* 33(5), pp. 1479-1490.

Kamba, T., Kanatani, H., and Tabuchi, M. (1991). "Strength and Rigidity of Joint Panel of Concrete Filled CHS Column-to-Beam Connections", *Proceedings of the Third International Conference on Steel-Concrete Composite Structures*, Wakabayashi, M. (ed.), Fukuoka, Japan, 1991, Association for International Cooperation and Research in Steel-Concrete Composite Structures, pp. 189-194.

Kawano, A. and Matsui, C. (1997). "New Connections Using Vertical Stiffeners Between Hshaped Beams and Hollow or Concrete-Filled Square Tubular Columns", Composite Construction in Steel and Concrete III, Buckner, C. D. and Shahrooz, B. M. (eds.), *Proceedings of the Engineering Foundation Conference*, Irsee, Germany, American Society of Civil Engineers, New York, pp. 172-185.

MacRae, G. A., Roeder, C. W., Gunderson, C. A., and Kimura, Y. (2004). "Brace-beam-column connections for concentrically braced frames with concrete filled tube columns", *Journal of Structural Engineering (ASCE)*, 130(2), pp. 233-243.

Mander, J. B., Priestley, M. J. N., and Park, R. (1988). "Theoretical Stress-Strain Model for Confined Concrete." *Journal of Structural Engineering*, ASCE, 114(8), pp. 1804-1826.

Peng, S., Ricles, J. M., and Lu, L. (2000). "Full-scale Testing of Seismically Resistant Moment Connections For Concrete-filled Tube Column-to-WF Beam Hybrid Systems," Composite and Hybrid Structures*, Proceedings of the Sixth ASCCS International Conference on Steel-Concrete Composite Structures*, Xiao, Y. and Mahin, S. A. (eds.), Los Angeles, California, Association for International Cooperation and Research in Steel-Concrete Composite Structures, Los Angeles, California, pp. 591-598.

Popovics, S. (1973). "A Numerical Approach to the Complete Stress-Strain Curve of Concrete." *Cement and Concrete Research*, 3(5), pp. 583-599.

Prion, H. G. L. and McLellan, Andrew B. (1992). "Connecting Steel Beams to Concrete-Filled Steel Columns," *Proceedings of the ASCE Tenth Structures Congress '92*, Morgan, J. (ed.), San mAntonio, Texas, American Society of Civil Engineers, New York, pp. 918-921.

Ramadan, H. M., Hassan, M. M., Mooty, M. A., and Mourad, S. A. (2016). "Finite element analysis of circular concrete filled tube connections." *Journal of Constructional Steel Research*, 120, pp. 33-44.

Ricles, J. M., Lu, L.-W., Graham, W. W., Jr., and Vermaas, G. W. (1997). "Seismic Performance of CFT Column-WF Beam Rigid Connections," Composite Construction in Steel and Concrete III, Buckner, C. D. and Shahrooz, B. M. (eds.), *Proceedings of the Engineering Foundation Conference,* Irsee, Germany, American Society of Civil

Engineers, New York, pp. 282-297.
Roeder, C. W. (2000). "Seismic behavior of steel braced frame connections to composite columns."*Connections in Steel Structure*, 4, pp. 51-62.
Sakino, K., Nakahara, H., Morino, S., and Nishiyama, I. (2004), "Behavior of centrally loaded concrete-filled steel-tube short columns", *Journal of Structural Engineering*, ASCE, 130(2), pp. 180-188.
Schneider, S. P. and Alostaz, Y. M. (1998). "Experimental Behavior of Connections to Concrete-Filled Steel Tubes," *Journal of Constructional Steel Research,* 45(3), pp. 321-352.
Shakir-Khalil, H. (1993a). "Pushout Strengths of Concrete-Filled Steel Hollow Sections," *The Structural Engineering,* 71(13), pp. 230-233.
Shakir-Khalil, H. (1993b). "Resistance of Concrete-Filled Steel Tubes to Pushout Forces," *The Structural Engineering,* 71(13), pp. 234-243.
Shakir-Khalil, H. (1994a). "Finplate Connections to Concrete-Filled Tubes," Steel-Concrete Composite Structures, *Proceedings of the Fourth International Conference on Steel-Concrete Composite Structures*, Javor, T. (ed.), Kosice, Slovakia, 20-23 June 1994, held by the Association for International Cooperation and Research in Steel-Concrete Composite Structures, Expertcentrum, Bratislava, Slovakia, pp. 181-185.
Shakir-Khalil, H. (1994b). "Beam Connections to Concrete-Filled Tubes", Tubular Structures VI, *Proceedings of the Sixth International Symposium on Tubular Structures*, Grundy, P., Holgate, A., and Wong, W. (eds.), Melbourne, Australia, 14-16 December 1994, A. A. Balkema, Rotterdam, The Netherlands, pp. 357-364.
Shakir-Khalil, H. and Mahmoud, M. A. (1995). "Steel Beam Connections to Concrete-Filled Tubular Columns," *Nordic Steel Construction Conference*, Sweden.
Shakir-Khalil, H. and Al-Rawdan, A. (1996). "Behavior of Asymmetrically Loaded Concrete-Filled Tubular Columns" Tubular Structures VII, *Proceedings of the Seventh International Symposium on Tubular Structures*, Farkas J. and Jarmai, K. (eds.), University of Miskolc, Hungary, August 28-30, 1996, pp. 363-370.
Susantha, K. A .S., Ge, H., and Usami, T. (2001). "Uniaxial stress-strain relationship of concrete confined by various shaped steel tubes", *Engineering Structures*, 23(10), 1331-1347.
Vulcu, C., Stratan, A., and Dubina, D. (2012). "Seismic resistant welded connections for MRF of CFT columns and I beams", *7th International Workshop on Connections in Steel Structures*, 30 May-02 June.
Yao, H., Goldsworthy, H., and Gad, E. (2008). "Experimental and Numerical Investigation of the Tensile Behavior of Blind-Bolted T-Stub Connections to Concrete-Filled Circular Columns." *J. Struct. Eng,* 2(198), pp. 198-208.
Zhang, J., Denavit, M. D., Hajjar, J. F., and Lu, X. (2012). "Bond Behavior of Concrete-Filled Steel Tube (CFT) Structures," *Engineering Journal*, AISC, 49(4), pp. 169-185.